OPEN ACCESS

University of BRISTOL

Jones, M. R. (2020). High-Pressure Modulation of Primary Photosynthetic Reactions. *Journal of Physical Chemistry B*, *2020*. https://doi.org/10.1021/acs.jpcb.9b09342

Peer reviewed version

Link to published version (if available):
10.1021/acs.jpcb.9b09342

Link to publication record in Explore Bristol Research
PDF-document

University of Bristol - Explore Bristol Research
General rights

High-Pressure Modulation of Primary Photosynthetic Reactions

SCHOLARONE™
Manuscripts

High-Pressure Modulation of Primary Photosynthetic Reactions

Erko Jalviste[a], Kõu Timpmann[a], Manoop Chenchiliyan[a], Liina Kangur[a], Michael R. Jones[b], and Arvi Freiberg[a, c, d] *

[a]Institute of Physics, University of Tartu, W. Ostwald Str. 1, Tartu 50411, Estonia

[b]School of Biochemistry, University of Bristol, Biomedical Sciences Building, University Walk, Bristol, BS8 1TD, United Kingdom

[c]Institute of Molecular and Cell Biology, University of Tartu, Riia 23, Tartu 51010, Estonia

[d]Estonian Academy of Sciences, Kohtu 6, 10130 Tallinn, Estonia

*Corresponding author: Tel: +37256453175, e-mail: arvi.freiberg@ut.ee

ABSTRACT: Photochemical charge separation is key to biological solar energy conversion. Although many features of this highly quantum-efficient process have been described, others remain poorly understood. Herein, ultrafast fluorescence barospectroscopy is used for the first time to obtain insights into the mechanism of primary charge separation in a YM210W mutant bacterial reaction center under novel surrounding modulating conditions. Over a range of applied hydrostatic pressures reaching 10 kbar the rate of primary charge separation monotonously increased and that of the electron transfer to secondary acceptor decreased. While the inferred free energy gap for charge separation generally narrowed with increasing pressure, a pressure-induced break of a protein-cofactor hydrogen bond observed at ~2 kbar significantly (by 219 cm^{-1} or 27 meV) increased this gap, resulting in a drop in fluorescence. The findings strongly favor a model for primary charge separation that incorporates charge recombination and restoration of the excited primary pair state, over a purely sequential model. We show that the main reason for the almost 3-fold acceleration of the primary electron transfer rate is the pressure-induced increase of the electronic coupling energy, rather than a change of activation energy. We also conclude that across all applied pressures the primary electron transfer in the mutant reaction center studied can be considered non-adiabatic, normal-region, and thermally activated.

Introduction

Electron transfer (ET) reactions are ubiquitous in nature underpinning key biological processes.[1-3] In photosynthesis, solar light energy is converted into chemical energy by a sequence of light-driven ET steps in a trans-membrane pigment-protein complex called the reaction center (RC). The accumulated potential energy of separated electrical charges across the membrane dielectric is then used to drive all subsequent cellular processes, powering most of the biosphere. In the relatively simple RC from the purple photosynthetic bacterium *Rhodobacter* (*Rba.*) *sphaeroides*, charge separation takes place on a time scale of a few picoseconds between a primary electron donor (P) formed from two closely interacting bacteriochlorophyll (BChl) molecules (P_A and P_B) forming the so-called special pair and a monomeric BChl acceptor (B_A). The electron is then passed to a bacteriopheophytin (BPhe, H_A), a primary acceptor ubiquinone (Q_A) and a secondary acceptor ubiquinone (Q_B), see inset of Figure 1A.[4] The mechanism of this highly quantum-efficient charge separation has been studied using ultrafast spectroscopy, with valuable contributions from site-directed mutagenesis to alter the structure or cofactor composition of the RC and low-temperature conditions to improve spectral resolution and modulate radical pair lifetimes.

While the sensitivity of ET processes in bacterial RCs to temperature is well known as well as at least qualitatively understood,[5-6] the response of the primary charge separation reactions to pressure, another important thermodynamic parameter, has not yet been characterized. Previous work on pressure modulation of RCs has focused on the effects of steady-state spectra or secondary (slow) electron transfer reactions where measurement of a sample under high pressure is less technically demanding.[7-13] However, it is to be expected that the rate of ultrafast primary charge separation will also be dependent on pressure as rates of electron transfer by a tunneling mechanism have been generally thought to depend exponentially on the distance between the atoms/molecules involved.[3,14-15] Such distances can be conveniently modulated by externally applied hydrostatic pressure; see refs 16-17 for experiments on artificially designed systems.

In this work the kinetic and energetic responses of primary charge separation in the *Rba. sphaeroides* RC to elevated pressure were characterized for the first time by picosecond time-resolved fluorescence barospectroscopy. High hydrostatic pressures reaching 10 kbar (1000 MPa) were applied at ambient temperature in order to modulate the primary reactions in a novel way.

An engineered RC was used in which a tyrosine (Y) residue at position M210 was replaced by a tryptophan (W).[18] This well-characterized YM210W modification slows primary charge separation by more than 20-fold,[19-22] creating a situation where the expected pressure-induced acceleration of this process can be conveniently studied over broader pressure range. Furthermore, slower charge separation results in stronger emission from the special pair prior the charge separation, improving the signal to noise ratio of the measurements. From a more fundamental point of view, the slowness of primary charge separation compared with major thermal relaxation processes observed in the YM210W RC may at least partially eliminate arguments raised in connection with wild type RCs that classical non-adiabatic models may not be adequate for description of primary photosynthetic ET steps and should be replaced by adiabatic model versions.[23]

With respect to the following discussion, two facts about the YM210W mutant are important to note. Firstly, as for the wild type RC, there is only a single modulating hydrogen bond (H-bond) between the special pair BChls (specifically P_A) and their protein surroundings. Secondly, in the mutant the primary charge separation rate decreases with lowering temperature,[19] suggesting a thermally activated ET. This is opposite to the activationless ET in the wild type RC, where the rate increases when the temperature decreases.[5]

One of the major technical challenges of *in vitro* ultrafast time-resolved measurements of RCs is possible imitation of *in vivo* conditions for ET with unrestricted flow of electrons through the RC. In natural photosynthesis, the special pair remains in an oxidized (P^+) state for a considerable amount of time following charge separation, and so is unable to accept further excitations. This defines the closed RC state. Subsequent reduction of the special pair via a cyclic electron transfer mechanism reactivates the RC with a typical rate of 10 s^{-1}.[24] To accelerate reduction of the special pair, and thereby improve the signal during *in vitro* measurements, external electron donors such as ascorbate are frequently used. However, in this case, electrons may start accumulating on the primary quinone acceptor, another adverse photo-induced effect. In the present work, the excitation light intensity was kept sufficiently low to avoid light-induced closing of RCs (see Figure S1 in Supporting Information (SI)), as first observed in intact bacterial membranes complete with light-harvesting and RC complexes[25] (reviewed in ref 26).

Materials and Methods

Samples. Purification of YM210W RC complexes for spectroscopic measurements was as described previously.[27-28] Protein samples were stored at –78°C until used. Defrosted concentrated samples were diluted before experiments with 20 mM Tris/0.04% β-DDM (pH 7.8) to obtain an optical density of ≤0.1 at P band maximum in the sample cell to avoid emission reabsorption effects. More concentrated samples (optical density up to 0.3) were used in some measurements to achieve a greater signal.

High-Pressure Measurements. A 0.35 mm thick stainless steel gasket with 0.3 mm diameter orifice was used to contain the sample between the anvils of a diamond anvil cell (DAC) (D-02, Diacell Products Ltd.), as recently described.[29-30] Pressure applied at an average rate of 6-20 MPa per minute was determined optically using a ruby-microbead pressure sensor (RSA Le Rubis SA) directly mounted into the sample volume. The precision of the pressure measurements was ±100-200 bar. The temperature of the DAC was maintained at 23±0.5°C using a Haake F3 thermostat.

Steady-State and Picosecond Time-Resolved Spectroscopy. Steady-state transmission and fluorescence spectra were measured with a resolution of 1 nm via a 0.3 m spectrograph (Shamrock SR-303i, Andor Technology) equipped with a thermo-electrically cooled CCD camera (DV420A-OE, Andor Technology), and a blackbody tungsten light source BPS100 (BWTek) or a Ti:sapphire laser (3900S, Spectra Physics). Fluorescence spectra were corrected for the spectral sensitivity of the set-up. Absorption spectra (A) were evaluated from the measured transmission spectra (T) as: A=−log(T). To obtain the relative peak shifts for absorption/emission spectra, first ambient pressure spectra were measured by placing the sample in a quartz cuvette at ambient pressure. Then the differences in peak position obtained at elevated pressures and at 1 bar were calculated.

Fluorescence decay kinetics were measured in transmission mode (i.e. exciting through the back side of the DAC and collecting the signal from its front face) with direct excitation into the low energy P absorbance band. A tunable femtosecond pulsed Ti:Sapphire laser (Coherent Mira Optima 900-F) with a pulse temporal/spectral width of 100 fs/15 nm and repetition rate of 3.8 MHz was used. No recording wavelength dependence of the kinetics was observed in control measurements performed at ambient pressure. Emission was thus recorded broadband, through a

4

long pass filter (TLP01-887, AHF Analysentechnik), using a time-correlated single photon counting system (SPC-150, Becker & Hickl GmbH) equipped with an avalanche photodiode (ID 100-50, ID Quantique). The fluorescence kinetics convoluted with the temporal response function of the set-up (see inset of Figure 2A) were analyzed by Spectra Solve (Version 2.0, LASTEK Pty. Ltd) software assuming multi-exponential decays.

Three to six independent measurements were carried out to ensure reproducibility of the data. No significant degradation of the sample during the data collection time (from tens of seconds to tens of minutes in different measurements) was observed. Reversibility of the system was confirmed by a recovery of the original spectra and kinetics upon the release of pressure.

**Results**

Impact of High Pressure on Steady-State Spectra. The absorption and emission spectra of YM210W RCs in near-infrared spectral range measured at low (100 bar) and high (2.4 kbar) pressures are shown in Figure 1A. The absorption spectra comprise three main bands associated with the Q_y transitions in the BChl and BPhe cofactors. The longest wavelength P band that at 1 bar peaks at 869 nm is ascribed to the lowest excitonic state of the special pair – a π-stacked structure of two BChl molecules (see Graphical Abstract), the B band at 807 nm to the two accessory BChls (including B_A), and the H band at 756 nm to the two BPhes (including H_A).[31] In the wild type RC the respective peaks are found at 868, 804 and 758 nm.[5]

In agreement with previous measurements with various RCs,[29-30] all three absorbance bands universally shifted towards longer wavelengths (red-shifted) and broadened with increasing pressure (Figure 1A). Since the emission of fully functional RCs is associated with the special pair, we will subsequently focus only on the effect of pressure on the P band.

As can be seen in Figure 1B, the pressure-induced shift of the P absorption and fluorescence band maxima plotted on an energy scale was far from monotonous. The initial almost linear red-shift in absorption (fluorescence) spectra was at ~1.5 (~2) kbar replaced by a blue-shift (absorption) or no shift (fluorescence), only to continue red-shifting again beyond ~3 kbar, albeit with a somewhat shallower dependence on pressure. This peculiar behavior, previously observed in several RCs, has been explained as being due to a pressure-induced rupture of an H-bond that

stabilizes the special pair in its protein binding pocket.[29–30] The present work thus corroborated this conclusion, although a discrepancy between precise courses of the absorption and fluorescence band shifts depicted in Figure 1B requires explanation, see below.
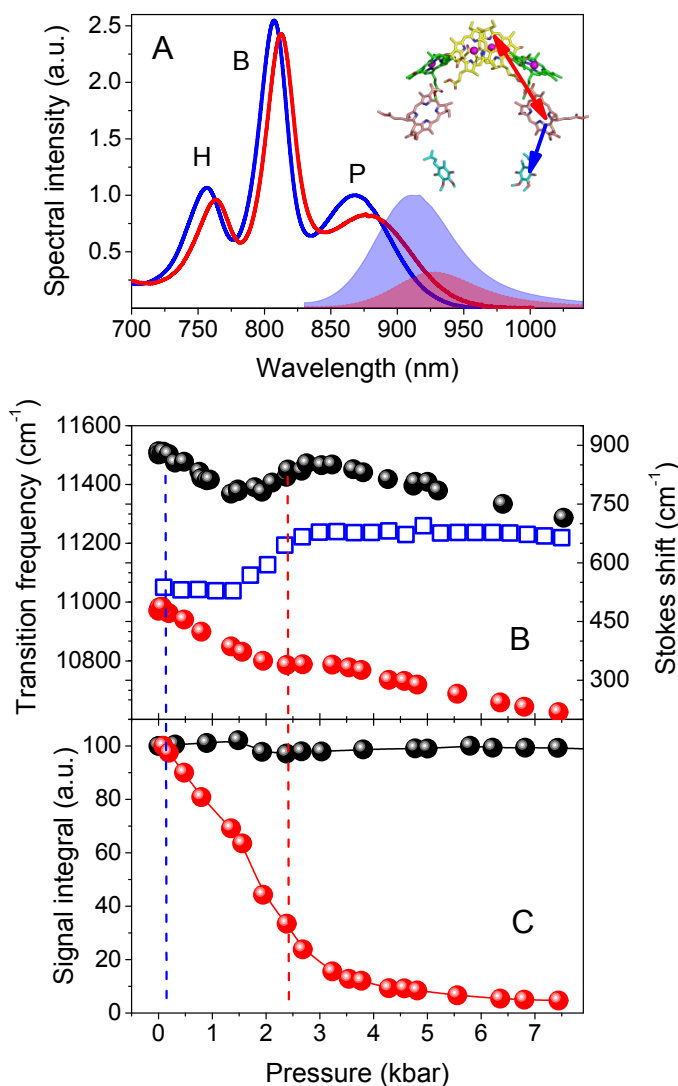
Figure 1. Impact of high pressure at ambient temperature on steady-state spectra of purified YM210W RC complexes. (A) Absorption (solid lines) and emission (filled shapes) spectra measured at 100 bar (blue) and 2.4 kbar (red). Common nomenclature of the separate pigment cofactor absorption bands of the RC is displayed. The emission was in response to excitation of the B absorption band at 806 nm. The inset shows the arrangement of cofactors (P – yellow, B – green, H – brown, Q – turquoise) in the RC with the main routes of electron transfer along the photo-chemically responsive (active or A) side of the RC structure. The red double arrow

designates forward and reverse electron transfers between the states P* (excited P) and $P^+H_A^-$ and the blue arrow, designates forward electron transfer from the $P^+H_A^-$ state to Q_A. (B) Pressure dependence of the P-band absorption (left axis, black balls) and emission (left axis, red balls) peak energies, and the Stokes shift (right axis, blue squares). (C) Integrated intensities of absorption (black) and emission (red) spectra as a function of pressure. The emission data were corrected for the pressure change of the absorbance at the excitation wavelength. Lines connecting data points are to lead the eye. Vertical dashed lines indicate the pressures at which the spectra shown in panel A were measured.

Shown also in Figure 1B is the pressure dependence of the energy difference between the absorption and emission peaks, a quality which in spectroscopy is called the Stokes shift. The Stokes shift can be considered as a measure of internal molecular dissipation of energy and environmental reorganization that accompany an electronic transition in a pigment chromophore (or system of coupled chromophores). In linear response theory, the Stokes shift equals two times the reorganization energy, subsequently labeled as λ. At low (≤1.5 kbar) and high (≥3.5 kbar) pressures the Stokes shift (and the underlying electron-nuclear coupling) is rather independent on pressure. In between, it abruptly increases. Although it is tempting to relate this growth just to a reorganization of the environment in response to the break of the H-bond, this is hardly the case because of the strong heterogeneity of the emissive properties of the sample.

Indeed, as demonstrated in Figure 1C, there was a strong loss of emission intensity of RCs at high pressures, in marked contrast to the absorbance integrated intensity that stayed practically constant. This loss of emission was reversible, its intensity almost completely recovering upon the release of pressure. We will further elaborate this issue below.

Dependence of Fluorescence Decay Kinetics on Pressure. As already mentioned, the emission from the YM210W mutant RC is relatively long-lived compared with that from the wild type RC due to the slowing of primary charge separation. Yet, as in the wild type RC, the decay of this emission is not mono-exponential. A good fit of the emission kinetics measured at 1 bar was obtained by applying a minimum of three exponentially decaying components with the following lifetimes τ and amplitudes A: $\tau_1 = 65.6$ ps and $A_1 = 86.8\%$; $\tau_2 = 178$ ps and $A_2 = 12.9\%$; $\tau_3 \sim 3000$ ps and $A_3 = 0.3\%$. The fastest component dominated the process and the slowest had a marginal (less than 1%) relative amplitude. These ambient-pressure excited state lifetimes

reasonably agree with the transient absorption spectroscopy data available in the literature, although quantitatively the latter lifetimes tend to be systematically shorter.[19-21]

According to Figure 2, the kinetics of emission decay significantly changed upon sample compression. The lifetime of the major component (τ_1) decreased almost exponentially, and was ~2.4 times shorter at 10 kbar than at 1 bar (Figure 2A). The lifetime of the intermediate component (τ_2) increased, but only by ~50% across the same pressure range (Figure 2B). The lifetime of the minor, 3 ns, component (not shown) was unchanged within experimental uncertainty.
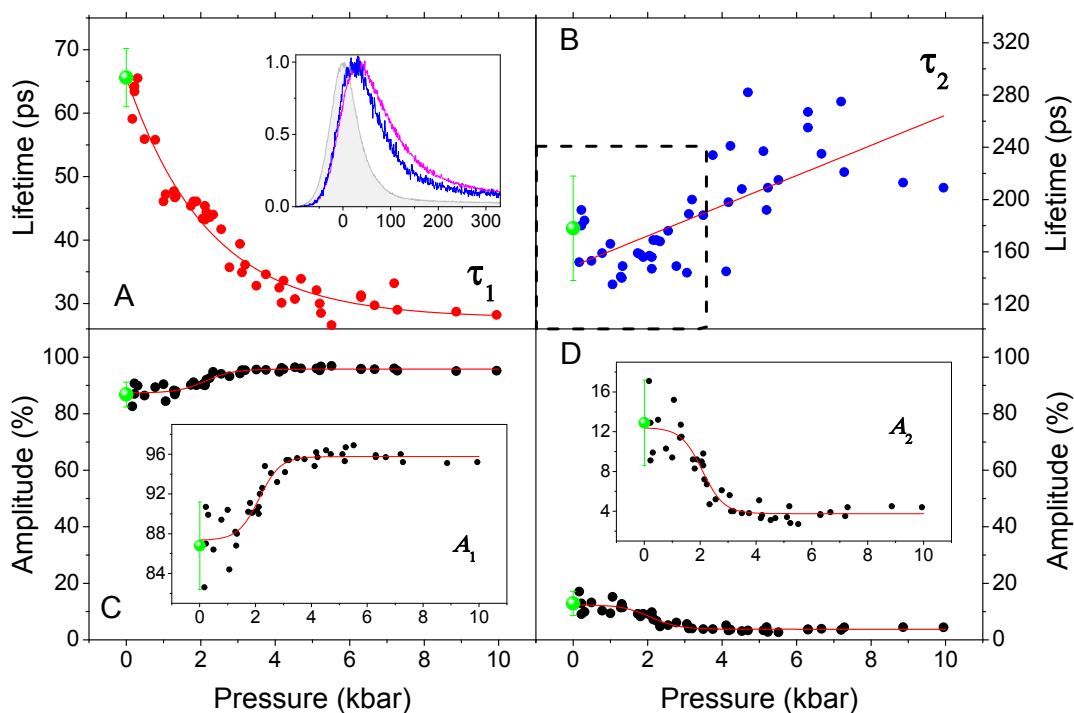
Figure 2. Pressure dependence of the RC picosecond fluorescence decay lifetimes (A, B) and related amplitudes (C, D). Scattered dots represent data from three independent measurements with 860-nm excitation, directly into the P absorption band. Thin red solid lines represent best fits of the experimental data. Green dots with uncertainty (mean squared deviation) denote averaged reference data measured at ambient pressure on 8 different (still as well as stirred) samples in a cuvette. Insets: (A) Fluorescence decay kinetics at 0.2 kbar (magenta) and 8.9 kbar (blue), and the related temporal response function of the instrument with ~70 ps full width at half maximum (grey filled shape). The amplified noise associated with the high-pressure curve reflects strong quenching of fluorescence at elevated pressures; (C, D) Vertically expanded views of the

corresponding main graphs. The dashed square in panel (B) demarcates the pressure range covered in previously published measurements of the secondary ET step.[9] See text for further explanations.

In previous pressure measurements limited to 3.5 kbar carried out on carotenoidless RCs from *Rba. sphaeroides* R-26 the rate of the $H_A^- \rightarrow Q_A$ ET step increased from $(218 \text{ ps})^{-1}$ at ambient pressure to $(152 \text{ ps})^{-1}$ at 2.4 kbar.[9] Upon further increase of pressure, the trend was reversed, the rate slowing to $(199 \text{ ps})^{-1}$ at 3.5 kbar. Although similar behavior is not excluded in our case (see dashed square in Figure 2B), the data are too noisy to be definitive on this point. Observing the data on the much broader scale of pressures applied in this work, it is quite clear that the main tendency of (τ_2) is a linear increase with pressure.

In contrast to the continuous trends observed for lifetimes τ_1 and τ_2, the associated amplitudes showed a stepwise variation between 1.5 and 3.5 kbar (Figures 2C and 2D). More detailed views of these steps, amounting to 8-9% of the amplitude, are shown in the insets to these Figures. Marking a boundary between the above low-pressure (<1.5 kbar) and high-pressure (>3 kbar) regions where the amplitudes were approximately constant, the steps designate opposite tendencies with A_1 increasing and A_2 decreasing. We further note that at high pressures the kinetics becomes almost single-exponential with the τ_1 component accounting for ~96% of the total amplitude.

The abrupt changes seen in the pressure dependencies of the steady-state spectral positions (Figures 1B and 1C) and of relative amplitudes of the time-resolved fluorescence decay components (Figures 2C and 2D) occurred at similar pressures, suggesting a common connection. Yet all the variations of lifetimes and amplitudes of the transient emission on increased pressure corresponded to only a two-fold decrease in integral intensity, which was at odds with the more than 10-fold loss in the integral intensity of the steady-state fluorescence demonstrated in Figure 1C. A recognition that the ensemble of purified RCs contains subpopulations with different endurance against pressure that manifests in their emission quenching properties[30] could solve this apparent contradiction. Figure 1C shows that quenching of the RC emission, which begins immediately after the pressure increase, accelerates at ~1 kbar, coincident with the initiation pressure of the H-bond break according to the absorption spectrum. The fact that emission from a special pair with a broken H-bond is significantly quenched explains the different course of the

fluorescence band position relative to that of the absorption band (Figure 1B). This is because although all RCs contribute to the absorption spectrum, only the most robust (least quenched) sub-population of RC contributes to the emission spectrum.

Discussion

Kinetic Model. A kinetic scheme given by eq 1 was used to model the decay of the electronically excited special pair state (P^*) via photochemical (charge separation) and non-photochemical (internal conversion, inter-system crossing and fluorescence) mechanisms. In contrast to the widely used purely sequential electron transfer scheme, it allows for an intermediate reverse reaction (charge recombination to the excited state) and, as a consequence, a delayed (recombination) fluorescence by repopulation of the P^* state. The strongest argument for inclusion of the charge recombination phase is the observed abrupt decrease of A_2, the amplitude of τ_2, which to our understanding is essentially related to the $P^+H_A^-$ state. As shown below, this relatively simple model was not only qualitatively but also quantitatively able to reproduce all of the above intricate experimental observations. The two-state (P^* and $P^+H_A^-$) model yielded two-exponential kinetics for decay of the P^* state population characterized by four rate constants, k_0, k_1, k_2, and k_3 (see SI for details):

$$\overset{k_0}{\leftarrow} P^* \underset{k_2}{\overset{k_1}{\rightleftharpoons}} P^+H^- \overset{k_3}{\rightarrow},$$

(1)

In the scheme of eq 1, the rate constant of $P^* \rightarrow P^+H_A^-$ charge separation is k_1, while further electron transfer to the first quinone acceptor is described by the rate constant k_3. Decay of the P^* state population by non-photochemical routes is described by a single rate constant k_0. Its value determined in modified RCs of *Rba. sphaeroides*[24] and *Rba. capsulatus*[32] varies between $(750\ ps)^{-1}$ and $(180\ ps)^{-1}$. In the latter case, it was explicitly noted that k_0 was exclusively determined by internal conversion to the ground state. The rate constant k_2 denotes the charge recombination process, $P^* \leftarrow P^+H_A^-$, explaining the observed non-monoexponential decay of P^*. This process normally proceeds uphill in energy and is made available by thermal bath activation. In the following the standard free energy difference between the P^+H^- and P^* states is referred to as the gap, $-\Delta G^0$.

This model obviously includes a few implicit assumptions. First, as is known from experiment, only the A branch of RC cofactors is active in the ET processes to any significant extent. Therefore, in the scheme defined by eq 1 and from now on, the branch subscripts will be dropped, unless absolutely required for clarity. Second, due to direct excitation into the low energy P absorption band, initially only the special pair first singlet excited state is populated, i.e. the initial concentration [P*] equals to 1. Third, the first experimentally distinguishable charge-separated state is P^+H^- as schematically indicated in inset of Figure 1A. This is because the intermediate P^+B^- state in the YM210W mutant RC is known to be energetically shifted close to (or even above) the P* state, and is hardly detectable as a separate state.[19,21-22]

Pressure Dependence of the Rate Constants and Free Energy Gap. Input parameters for calculations based on scheme (1) were the experimental lifetimes τ_1 and τ_2, the relative amplitudes A_1 and A_2 determined at each pressure, and a fixed-value non-photochemical decay rate constant k_0 (see below). A contribution from the τ_3 decay component was ignored due to its negligible amplitude and impartiality on pressure. Due to the normalization condition, $\sum_i A_i = 1$, the number of independent input parameters is reduced to six.

To curtail experimental noise, the scattered data sets shown in Figure 2 were fitted to a single-exponential function with a constant background for the data in Figure 2A, a linear function for the data in Figure 2B, and a sigmoidal function, $(a_1 - a_2)/\left(1 - \exp\left[\frac{p - p_c}{\delta}\right]\right) + a_2$, with parameters a_1, a_2, p_c and δ for the data in Figures 2C and 2D. k_0 in the YM210W mutant is not known, nor is its pressure dependence. However, its value at ambient conditions can be approximately estimated from the quantum yield of primary ET determined in ref 19 to be equal to 0.8 and from the present fluorescence lifetime measurements. These considerations yielded k_0 = (330 ps)$^{-1}$. Because the calculations showed qualitatively (and even quantitatively, as long as k_0 is not close to k_1) rather limited sensitivity with respect to this parameter (see Figure S2), k_0 was considered to be constant across the whole pressure range.

The results of calculation in Figure 3 imply that pressure has a strong impact on all three calculated rate constants. However, while the pressure dependence of the constants that describe forward electron transfers, k_1 (Figure 3A) and k_3 (Figure 3C), are smooth, the constant k_2 related to charge recombination (Figure 3B) appears complex, following an interrupted course. This rate

accelerates with increasing pressure both at low and high pressures, but suffers a significant (~55%) slow down between 2-3 kbar, the same pressure region where the breakage of the H-bond related to special pair takes place according to steady-state spectroscopy results, see above.
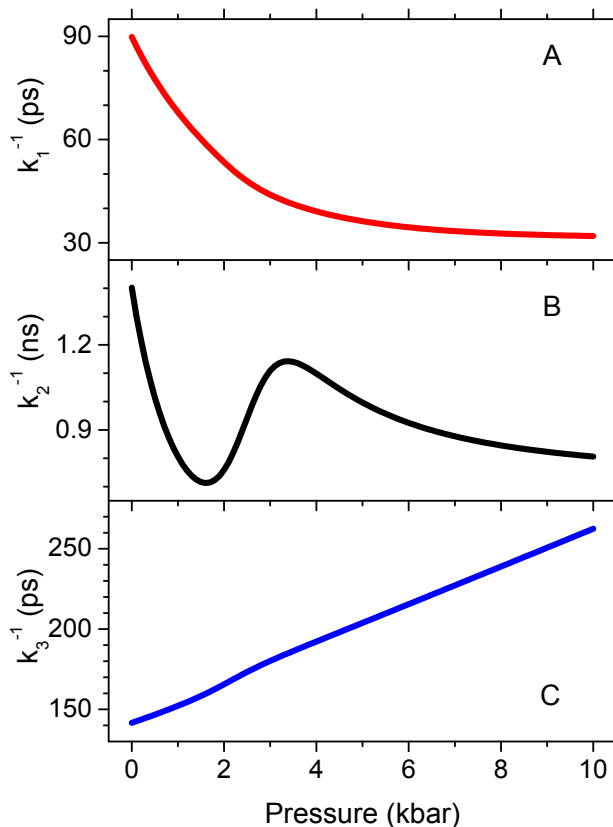
Figure 3. Simulated pressure dependences of inverse rate constants according to eq 1. A constant $k_0^{-1} = 330$ ps was used. See text for further explanation.

Assuming thermal equilibrium, a free energy gap $-\Delta G^0$ between the P^+H^- and P^* states and its pressure dependence can be derived applying eq 2 from the pressure dependent rate constants of experimental kinetics, $k_1 = k_1(p)$ and $k_2 = k_2(p)$:

$$-\Delta G^0 = RT\ln\frac{[P^+H^-]}{[P^*]} = RT\ln\frac{k_1}{k_2}. \tag{2}$$

In eq 2, $[P^*]$ and $[P^+H^-]$ are the steady-state populations of initial and final states, R is the universal gas constant and T is the absolute temperature.

As can be seen in Figure 4, assuming $k_0^{-1} = 330$ ps, the calculated at 1 bar value of the gap equals $-\Delta G^0(1\ \text{bar}) = 569\ \text{cm}^{-1}$ (~71 meV). Reasonable variation of k_0^{-1} between the values of 750 ps [24] and 200 ps [32] allow deviations of the gap within a relatively narrow range of about $\pm 80\ \text{cm}^{-1}$ (Figure S2). The evaluated in this work gap size is thus within about 40% of that previously reported in the literature, $1008\pm40\ \text{cm}^{-1}$ (125 ± 5 meV), for the same type of RC but using a transient absorption technique.[19]
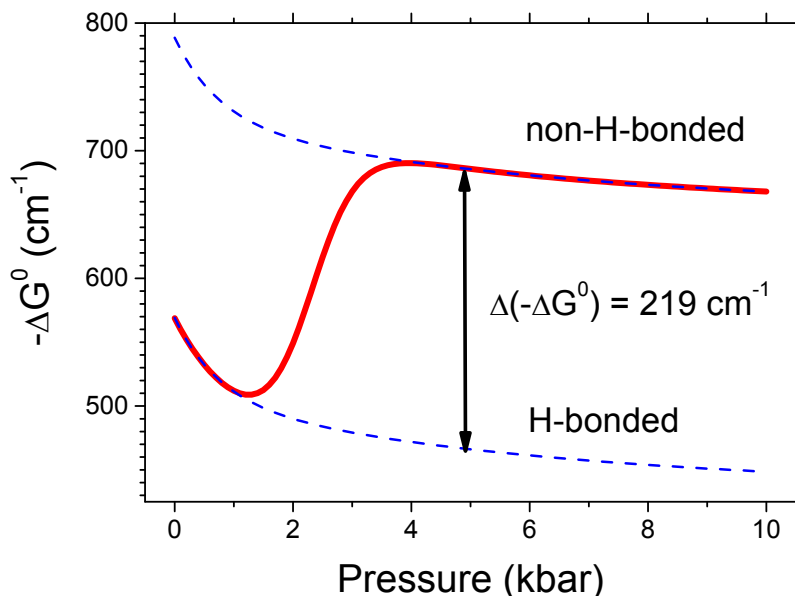
Figure 4. Simulated pressure dependence of the reaction free energy gap (solid red line). Blue dashed curves represent two identical functions shifted by 219 cm^{-1} with respect to each other along vertical axis. These model curves fit the low-pressure (lower energy curve) and high-pressure (higher energy curve) parts of the dependence. See text for further explanation.

Several factors may have contributed to this discrepancy, such as an incomplete relaxation of the P^+H^- state within the experimental time-window of the present measurements[23,33] as well as the above heterogeneity of the sample ensemble with respect to ET rate and their susceptibility to pressure. The differences observed in recombination dynamics of P^+H^- when detected in inhomogeneous systems by delayed emission or transient absorption is a longstanding issue, see,

13

e.g., refs 34-36. As explained in ref 35, the reason is that the kinetics observed in emission are determined by the high-energy tail of the inhomogeneous distribution of energy gaps, while absorption reflects the bulk average of the distribution.

Upon compression, the gap initially decreases with a relatively high rate of about -92 cm^{-1}/kbar. Then, at ~1.5 kbar, the trend reverses and $-\Delta G^0$ begins to stepwise rise before decreasing again past ~3.5 kbar. This latter decrease is, however, relatively small: -5.2 cm^{-1}/kbar at 5 kbar, for example.

It was observed that except the narrow step area, the dependence $-\Delta G^0 = -\Delta G^0(p)$ both at low and high pressures could be well approximated by the same exponentially decaying function of form $-\Delta G^0(p) = a + b\exp(-cp) + d\exp(-ep)$, properly shifted along vertical axis (a, *b, c, d, e* are the fitting constants and *p* is the pressure). This unique feature allows a solid determination of the change of the free energy gap in response to breaking of the lone H-bond that stabilizes special pair in the RC protein structure: $\Delta(-\Delta G^0) = 219 \pm 4$ cm^{-1}. It should be noted that this energy change is not a measure of the H-bond energy. The latter, as estimated from the shift of steady-state absorption spectra and using the methodology described in ref 29, equals to 15-16 kJ/mol (1250-1340 cm^{-1}).

Analysis of the Primary Electron Transfer Process as a Function of Pressure. In the following the pressure dependence of k_1 – the primary ET rate constant – is analyzed using weak coupling Marcus theory.[3,37] This rate between a donor molecule/initial state (here P*H) and acceptor molecule/final state (here P$^+$H$^-$) is given by

$$k_1 = V^2 \sqrt{\frac{4\pi^3}{h^2} \cdot \frac{1}{\lambda k_B T}} \exp\left[-\frac{\left(\Delta G^0 + \lambda\right)^2}{4\lambda k_B T}\right], \tag{3}$$

where V is the electronic coupling matrix element between the initial and final states, and h and k_B are, correspondingly, the Planck constant and the Boltzmann constant. The terms $E_a = (\Delta G^0 + \lambda)^2/4\lambda$ and $k_B T$ in the exponent designate the activation free energy of the ET reaction and the average thermal energy at the temperature T, respectively. See Figure 5A for definition of the parameters.
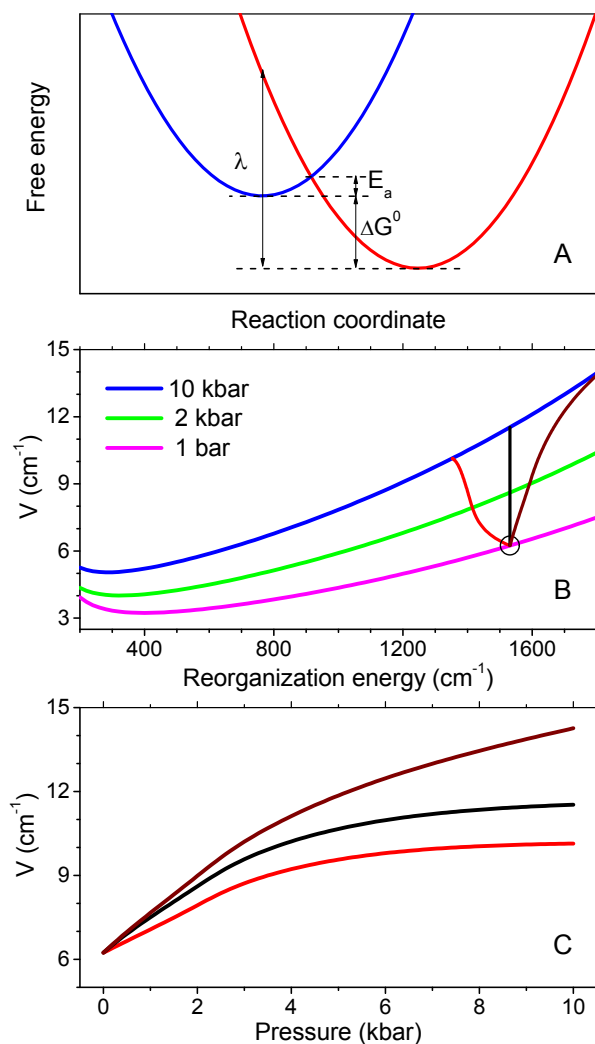
Figure 5. (A) Schematic illustration of the main model parameters according to Marcus theory, where the shifted potential energy curves represent initial (blue, P*H) and final (red, P$^+$H$^-$) states of primary ET. (B) Calculated relationships between the electronic coupling energy V and reorganization energy λ at the selected pressures indicated. The circle designates the derived value of reorganization energy at ambient pressure, while colored lines trace its change with pressure under the following restrictions: $\lambda(p)$ = const. (black), $E_a(p)$ = const. (red), and $\lambda(p) = \lambda(1$ bar$) + 30p$ (wine). (C) Pressure dependence of V under the above restrictions. Data in panels B and C are based on eq 3 but represent the (hypothetical) case of RCs with intact H-bond across all pressures. See text and Table 1 for further explanations.

Equation 3 is valid under the conditions that $2V/\lambda << 1$ and $V << h\langle\upsilon\rangle$, where $\langle\upsilon\rangle$ denotes an effective vibrational frequency coupled to ET. It is frequently taken that $h\langle\upsilon\rangle \approx 100$ cm^{-1}.[38] Physically, these limits adopt that vibrational equilibrium is established prior the ET takes place.

15

When the quantum nature of vibrations can be neglected that is a reasonable approximation at ambient temperature and normal region of ET, the donor and acceptor state free energies can be described classically, as quadratic functions of the reaction coordinate in harmonic approximation. Assuming similar coordinate dependence in initial and final states, and linear coupling between them, the ET results only in a relative shift along the reaction coordinate of the free energy parabolas representing initial and final states. The reorganization energy λ is then defined as the energy difference between the final state energy calculated at the equilibrium configuration of the initial state and the minimum of the final state, see Figure 5A. The ET rate is maximal when $\lambda = -\Delta G^0$; at which point the exponential factor in eq 3 equals 1.

The pressure dependencies of k_1 and ΔG^0 deduced from experiments do not allow unique determination either the electronic coupling energy V or reorganization energy λ. Yet taking advantage of the known temperature dependence of the P* decay rate,[19] which provides an ET activation energy $E_a(1\ \text{bar}) = 151\ \text{cm}^{-1}$, it is possible (ignoring plausible temperature dependence of the parameters) to evaluate λ at ambient pressure as follows: $\lambda(1\ \text{bar}) = 1530\ \text{cm}^{-1}$ (0.19 eV). This value practically coincides with that of a theoretical estimate (0.2 eV) based on straightforward electrostatic modeling.[39] We note in passing that in the context of the above discrepancy between the free energy gaps determined by different experimental methods, this agreement of the experimental and theoretical reorganization energies seem to dismiss incomplete relaxation in favor of the second explanation related to heterogeneity of the sample. Then, applying eq 3, one also obtains an assessment of the ambient-pressure electronic coupling energy: $V(1\ \text{bar}) = 6.2\ \text{cm}^{-1}$, see Table 1.

In order to illustrate the range of $V(p)$ and $\lambda(p)$ variations confined by eq 3 and the experimental $k_1(p)$ (Figure 3A) and $-\Delta G^0(p)$ (Figure 4) data, plotted in Figure 5B are $V(\lambda)$ dependences at the three arbitrarily chosen pressure values: 1 bar, 2 kbar and 10 kbar. The corresponding $-\Delta G^0(p)$ values have been obtained from Figure 4. For simplicity, just the lower branch of the $-\Delta G^0(p)$ fitting curve in Figure 4 was used, which relates to a (hypothetical) RC sample with intact H-bond across all pressures. Applying the upper branch related to a non-H-bonded RC provides qualitatively similar results. The $V(\lambda)$ curves in Figure 5B show minima in the 250 - 400 cm^{-1} region where $\lambda \sim -\Delta G^0$. This is in agreement with Marcus theory, where smaller and larger λ values compared with $-\Delta G^0$ correspond to the inverted and normal range of ET,

respectively. Because $-\Delta G^0$ generally diminishes with pressure (Figure 4), the minimum of $V(\lambda)$ shifts toward lower reorganization energy at higher pressures.

Pressure dependence of the reorganization energy is not experimentally known. Yet from theoretical grounds this dependence is expected to be weaker than that of $\Delta G^0(p)$.[15,40] This notion is indirectly supported by the practical independence on pressure of the Stokes shift in optical spectra observed in Figure 1B at both low- and high-pressure ranges. Therefore, we first analyzed a limit of reorganization energy that was independent of pressure: $\lambda = \lambda(p) = $ const. This case is in Figure 5B represented by vertical black line. The pressure dependence of electronic coupling energy when this restriction applies is shown by the black line in Figure 5C. Another model cases we looked at were $E_a = $ const. (corresponding to a decrease of λ with pressure) and $\lambda(p) = \lambda(1 \text{ bar})$ $+ 30p$ (corresponding to a linear increase of λ on pressure with a rate of 30 cm^{-1}/kbar). In Figures 5B and 5C these cases are signified by the red and wine lines, respectively, see also Figure S3B. There are of course many more options, but these specific examples are probably sufficient for a qualitative characterization of the complex interplay of V and λ as a function of pressure.

Table 1. Model parameters evaluated at 1 bar and 10 kbar.[a]

Parameter (cm^{-1})	@ 1 bar	@ 10 kbar		
		$\lambda = $ const.	$E_a = $ const.	$\lambda = \lambda(1 \text{ bar}) + 30p$
$-\Delta G^0$	569	449	449	449
E_a	151	191	151	261
λ	1530	1530	1350	1830
V	6.2	11.5	10.1	14.3

[a] The values at 10 kbar are evaluated for the H-bonded branch of the pressure dependence of $-\Delta G^0$ (see Figure 4) assuming three predefined dependences of λ on pressure.

In all cases examined, V predictably increases upon compression, albeit to a different degree (see Figure 5C and Table 1). Noteworthy, however, is the fact that instead of increasing

exponentially with pressure, as expected from naive single-coordinate models,[14] V tends to saturate at higher pressures. This tendency holds as long as the increase rate of λ is less than ~117 cm^{-1}/kbar. An analysis provided in the SI shows that allowance of an exponential growth of V with pressure is liable to produce an unphysical pressure dependence of the reorganization energy, characterized with an initial decrease of λ with pressure followed by an increase, see Figure S3. We thus conclude that a single-axis compression of the donor-acceptor distance is not a truthful model of ET processes in the RC protein structure under hydrostatic pressure. This important qualitative result deserves further elaboration based on real spatial structure of the RC. Similar nontrivial behavior concerning high-pressure compression of the RC special pair was observed in ref 13.

5. Summary and Conclusions

In this work, the response of primary photochemistry in the YM210W mutant RC complex of *Rba. sphaeroides* to hydrostatic compression was investigated. The mutant exhibits a slowed primary charge separation time that allows detailed studies of the kinetics of charge separation by a sensitive picosecond time-resolved single-photon counting technique. The experimental data obtained at ambient temperature and various pressures up to 10 kbar were analyzed using a two-level kinetic scheme involving primary charge separation described by the rate constant k_1, charge recombination to the initial excited state (k_2), electron transfer to a secondary electron acceptor (k_3), and direct (non-photochemical) quenching of the special pair (k_0). Significant effects of pressure were detected on all the rate constants as well as on the free energy gap associated with the primary ET ($-\Delta G^0$), with k_1 and k_2 generally increasing, and k_3 and $-\Delta G^0$ decreasing. The most striking observation was a sudden interruption of the change in k_2 and $-\Delta G^0$ taking place at ~2 kbar, in obvious correlation with the pressure-induced break of a lone H-bond between one of the special pair BChls (P_A) and the surrounding protein scaffold. By considerably increasing the free energy gap, this break is the basis of the three-fold drop in the recombination luminescence demonstrated in Figure 2D. This work thus strongly favors an ET model for bacterial RCs that involves reversible charge transfer over a wholly sequential model.

An acceleration of primary ET (increase of rate k_1) by pressure was thereafter analyzed using a classical Marcus model. The results of this investigation (see Table 1) implied that across

all pressures the primary ET process that takes place in this mutant RC at ambient temperature can be classified as nonadiabatic, thermally activated, and normal. The latter conclusion corroborates with the general notion, that, except in Photosystem I of oxygen-evolving organisms, inverted-region ET is not an important mechanism in photosynthetic photosystems.[41]

Despite remaining uncertainty about the pressure dependence of the reorganization energy, one can firmly conclude based on the data in Figure 5C that the main reason for the almost 3-fold acceleration of the primary ET rate (Figure 3A) is the pressure-induced increase of the electronic coupling energy, rather than change of the exponential Franck-Condon term in the Marcus equation (eq 3). One of the most promising experimental approaches to find out pressure dependence of the ET reorganization energy in photosynthetic RCs would be the measurement of RC emission kinetics as a function of temperature at series of pressures, analyzing the data obtained at each pressure with respect to λ, as was done above just at ambient pressure.

Emission from the RC was strongly yet reversibly quenched by breakage of the single H-bond between a special pair BChl and the surrounding protein. One thus has to conclude a substantial change in the electronic structure of the special pair (if not the whole RC) following the breakage of this local H-bond. The related structural details as well as mechanistic aspects of the pressure-induced H-bond break remain to be studied using more involved theoretical[42-44] and experimental methods.

Supporting Information. The material supplied as SI includes following parts: Excitation light intensity dependence of the RC emission; solution of the kinetic model; effect of k_0 on rate constants and free energy gap of ET; pressure-induced modifications of the electronic coupling and reorganization energy in consistence with the experimental change of the primary ET rate.

Acknowledgements

References

(1) Blumberger, J. Recent Advances in the Theory and Molecular Simulation of Biological Electron Transfer Reactions. *Chem. Rev.* **2015,** *115*, 11191-11238.

(2) Wörner, H. J.; Arrell, C. A.; Banerji, N.; Cannizzo, A.; Chergui, M.; Das, A. K.; Hamm, P.; Keller, U.; Kraus, P. M.; Liberatore, E., et al. Charge Migration and Charge Transfer in Molecular Systems. *Struct. Dyn.* **2017,** *4*, 061508.

(3) Marcus, R. A.; Sutin, N. Electron Transfers in Chemistry and Biology. *Biochim. Biophys. Acta* **1985,** *811*, 265-322.

(4) Williams, J. C.; Steiner, L. A.; Feher, G. Primary Structure of the Reaction Center from *Rhodopseudomonas Sphaeroides. Proteins: Struct., Funct., Genet.* **1986,** *1*, 312-325.

(5) Hoff, A. J.; Deisenhofer, J. Photophysics of Photosynthesis. Structure and Spectroscopy of Reaction Centers of Purple Bacteria. *Phys. Rep.* **1997,** *287*, 1-247.

(6) Renger, T. Theory of Optical Spectra Involving Charge Transfer States: Dynamic Localization Predicts a Temperature Dependent Optical Band Shift. *Phys. Rev. Lett.* **2004,** *93*, 188101.

(7) Clayton, R. K.; Devault, D. Effects of High Pressure on Photochemical Reaction Centers from *Rhodopseudomonas Spheroides. Photochem. Photobiol.* **1972,** *15*, 165-175.

(8) Windsor, M. W.; Menzel, R. Effect of Pressure on the 12 Ns Charge Recombination Step in Reduced Bacterial Reaction Centers of *Rhodobacter Sphaeroides* R-26. *Chem. Phys. Lett.* **1989,** *164*, 143-150.

(9) Redline, N. L.; Windsor, M. W.; Menzel, R. The Effect of Pressure on the Secondary (200 ps) Charge Transfer Step in Bacterial Reaction Centers of *Rhodobacter Sphaeroides* R-26. *Chem. Phys. Lett.* **1991,** *186*, 204-209.

(10) Redline, N. L.; Windsor, M. W. The Effect of Pressure on Charge Separation in Photosynthetic Bacterial Reaction Centers of *Rhodopseudomonas Viridis. Chem. Phys. Lett.* **1992,** *198*, 334-340.

(11) Gall, A.; Ellervee, A.; Bellissent-Funel, M.-C.; Robert, B.; Freiberg, A. Effect of High Pressure on the Photochemical Reaction Center from *Rhodobacter Sphaeroides* R26.1. *Biophys. J.* **2001,** *80*, 1487-1497.

(12) Gall, A.; Ellervee, A.; Robert, B.; Freiberg, A. The Effect of Internal Voids in Membrane Proteins: High-Pressure Study of Two Photochemical Reaction Centers from *Rhodobacter Sphaeroides. FEBS Lett.* **2004,** *28121*, 1-5.

(13) Leiger, K.; Freiberg, A.; Dahlbom, M. G.; Hush, N. S.; Reimers, J. R. Pressure-Induced Spectral Changes for the Special-Pair Radical Cation of the Bacterial Photosynthetic Reaction Center. *J. Chem. Phys.* **2007,** *126*, 215102.

(14) Page, C. C.; Moser, C. C.; Chen, X.; Dutton, P. L. Natural Engineering Principles of Electron Tunnelling in Biological Oxidation-Reduction. *Nature* **1999,** *402*, 47-52.

(15) Miyashita, O.; Go, N. Pressure Dependence of Protein Electron Transfer Reactions: Theory and Simulation. *J. Phys. Chem. B* **1999,** *103*, 562-571.

(16) Freiberg, A.; Ellervee, A.; Tars, M.; Timpmann, K.; Laisaar, A. Electron Transfer and Electronic Energy Relaxation under High Hydrostatic Pressure. *Biophys. Chem.* **1997,** *68*, 189-205.

(17) Tars, M.; Ellervee, A.; Wasielewski, M. R.; Freiberg, A. Biomolecular Electron Transfer under High Hydrostatic Pressure. *Spectrochim. Acta, Part A* **1998,** *54A*, 1177-1189.

(18) McAuley, K. E.; Fyfe, P. K.; Cogdell, R. J.; Isaacs, N. W.; Jones, M. R. X-Ray Crystal Structure of the YM210W Mutant Reaction Centre from *Rhodobacter Sphaeroides. FEBS Lett.* **2000,** *467*, 285-290.

(19) Nagarajan, V.; Parson, W. W.; Davis, D.; Schenck, C. C. Kinetics and Free Energy Gaps of Electron-Transfer Reactions in *Rhodobacter Sphaeroides* Reaction Centers. *Biochemistry* **1993,** *32*, 12324-12336.

(20) Beekman, L. M. P.; van Stokkum, I. H. M.; Monshouwer, R.; Rijnders, A. J.; McGlynn, P.; Visschers, R. W.; Jones, M. R.; van Grondelle, R. Primary Electron Transfer in Membrane-Bound Reaction Centers with Mutations at the M210 Position. *J. Phys. Chem.* **1996,** *100*, 7256-7268.

(21) Pawlowicz, N. P.; van Stokkum, I. H. M.; Breton, J.; van Grondelle, R.; Jones, M. R. An Investigation of Slow Charge Separation in a Tyrosine M210 to Tryptophan Mutant of the *Rhodobacter Sphaeroides* Reaction Center by Femtosecond Mid-Infrared Spectroscopy. *Phys. Chem. Chem. Phys.* **2010,** *12*, 2693-2705.

(22) Dominguez, P. N.; Himmelstoss, M.; Michelmann, J.; Lehner, F. T.; Gardiner, A. T.; Cogdell, R. J.; Zinth, W. Primary Reactions in Photosynthetic Reaction Centers of *Rhodobacter Sphaeroides* – Time Constants of the Initial Electron Transfer. *Chem. Phys. Lett.* **2014,** *601*, 103-109.

(23) Wang, H.; Lin, S.; Allen, J. P.; Williams, J.-A. C.; Blankert, S.; Lasr, C.; Woodbury, N. W. Protein Dynamics Control the Kinetics of Initial Electron Transfer in Photosynthesis. *Science* **2007,** *316*, 747-750.

(24) Müller, P.; Bieser, G.; Hartwich, G.; Langenbacher, T.; Lossau, H.; Ogrodnik, A.; Michel-Beyerle, M.-E. The Internal Conversion Rate of the Primary Donor in Reaction Centers of *Rhodobacter Sphaeroides*. *Ber. Bunsenges. Phys. Chem.* **1996,** *100*, 1967-1973.

(25) Borisov, A. Y.; Freiberg, A. M.; Godik, V. I.; Rebane, K.; Timpmann, K. Kinetics of Picosecond Bacteriochlorophyll Luminescence in Vivo as a Function of the Reaction Center State. *Biochim. Biophys. Acta, Bioenerg.* **1985,** *807*, 221-229.

(26) Valkunas, L.; Liuolia, V.; Freiberg, A. Picosecond Processes in Chromatophores at Various Excitation Intensities. *Photosynth. Res.* **1991,** *27*, 83-95.

(27) McAuley-Hecht, K. E.; Fyfe, P. K.; Ridge, J. P.; Prince, S. M.; Hunter, C. N.; Isaacs, N. W.; Cogdell, R. J.; Jones, M. R. Structural Studies of Wild-Type and Mutant Reaction Centers from an Antenna-Deficient Strain of *Rhodobacter Sphaeroides*: Monitoring the Optical Properties of the Complex from Bacterial Cell to Crystal. *Biochemistry* **1998,** *37*, 4740-4750.

(28) Jones, M. R.; Visschers, R. W.; van Grondelle, R.; Hunter, C. N. Construction and Characterization of a Mutant of *Rhodobacter Sphaeroides* with the Reaction Center as the Sole Pigment-Protein Complex. *Biochemistry* **1992,** *31*, 4458-4465.

(29) Kangur, L.; Jones, M. R.; Freiberg, A. Hydrogen Bonds in the Vicinity of the Special Pair of the Bacterial Reaction Center Probed by Hydrostatic High-Pressure Absorption Spectroscopy. *Biophys. Chem.* **2017,** *231*, 27-33.

(30) Timpmann, K.; Kangur, L.; Lõhmus, A.; Freiberg, A. High-Pressure Modulation of the Structure of the Bacterial Photochemical Reaction Center at Physiological and Cryogenic Temperatures. *J. Phys. B: At., Mol. Opt. Phys.* **2017,** *50*, 144006.

(31) van Brederode, M. E.; Jones, M. R.; van Grondelle, R. Fluorescence Excitation Spectra of Membrane-Bound Photosynthetic Reaction Centers of *Rhodobacter Sphaeroides* in Which the Tyrosine M210 Residue Is Replaced by Tryptophan: Evidence for a New Pathway of Charge Separation. *Chem. Phys. Lett.* **1997,** *268*, 143-149.

(32) Chuang, J. I.; Boxer, S. G.; Holten, D.; Kirmaier, C. High Yield of M-Side Electron Transfer in Mutants of *Rhodobacter Capsulatus* Reaction Centers Lacking the L-Side Bacteriopheophytin. *Biochemistry* **2006,** *45*, 3845-3851.

(33) Peloquin, J. M.; Williams, J. C.; Lin, X.; Alden, R. G.; Murchison, H. A.; Taguchi, A. K. W.; Allen, J. P.; Woodbury, N. W. Time-Dependent Thermodynamics During Early Electron Transfer in Reaction Centers from *Rhodobacter Sphaeroides*. *Biochemistry* **1994,** *33*, 8089-8100.

(34) Müller, M. G.; Griebenow, K.; Holzwarth, A. R. Primary Processes in Isolated Bacterial Reaction Centers from *Rhodobacter Sphaeroides* Studied by Picosecond Fluorescence Kinetics. *Chem. Phys. Lett.* **1992,** *199*, 465-469.

(35) Ogrodnik, A.; Keupp, W.; Volk, M.; Aumeier, G.; Michel-Beyerle, M. E. Inhomogeneity of Radical Pair Energies in Photosynthetic Reaction Centers Revealed by Differences in Recombination Dynamics of $P^+H_A^-$ When Detected in Delayed Emission and in Absorption. *J. Phys. Chem.* **1994,** *98*, 3432-3439.

(36) Ogrodnik, A.; Hartwich, G.; Lossau, H.; Michel-Beyerle, M. E. Dispersive Charge Separation and Conformational Cooling of $P^+H_A^-$ in Reaction Centers of *Rb. Sphaeroides* R26: A Spontaneous Emission Study. *Chem. Phys.* **1999,** *244*, 461-478.

(37) May, V.; Kühn, O. *Charge and Energy Transfer Dynamics in Molecular Systems*. Wiley-VCH: Berlin, 2000.

(38) Bixon, M.; Jortner, J.; Michel-Beyerle, M. E. A Kinetic Analysis of the Primary Charge Separation in Bacterial Photosynthesis. Energy Gaps and Static Heterogeneity. *Chem. Phys.* **1995,** *197*, 389-404.

(39) Krishtalik, L. I. Intramembrane Electron Transfer: Processes in the Photosynthetic Reaction Center. *Biochim. Biophys. Acta, Bioenerg.* **1996,** *1273*, 139-149.

(40) Manjari, S. R.; Kim, H. J. Temperature- and Pressure-Dependence of the Outer-Sphere Reorganization Free Energy for Electron Transfer Reactions: A Continuum Approach. *J. Phys. Chem. B* **2006,** *110*, 494-500.

(41) Makita, H.; Hastings, G. Inverted-Region Electron Transfer as a Mechanism for Enhancing Photosynthetic Solar Energy Conversion Efficiency. *Proc. Natl. Acad. Sci. U. S. A.* **2017,** *114*, 9267-9272.

(42) Matyushov, D. V. Protein Electron Transfer: Dynamics and Statistics. *J. Chem. Phys.* **2013,** *139*, 025102.

(43) Linnanto, J.; Freiberg, A.; Korppi-Tommola, J. Quantum Chemical Simulations of Excited-State Absorption Spectra of Photosynthetic Bacterial Reaction Center and Antenna Complexes. *J. Phys. Chem. B* **2011,** *115*, 5536-5544.

(44) Rafiq, S.; Scholes, G. D. From Fundamental Theories to Quantum Coherences in Electron Transfer. *J. Am. Chem. Soc.* **2019,** *141*, 708-722.

1
2
3
4
5
6
7
8
9
10
11
12
13
14
15
16
17
18
19
20
21
22
23
24
25
26
27
28
29
30
31
32
33
34
35
36
37
38
39
40
41
42
43
44
45
46
47
48
49
50
51
52
53
54
55
56
57
58
59
60

TOC Graphic